

# Comparison of Simple Algorithms for Estimating Respiration Rate from Electrical Impedance Pneumography Signals in Wearable Devices

Vala Jeyhani <sup>1</sup>, Tiina Vuorinen <sup>2</sup>, Matti Mäntysalo <sup>2</sup>, Antti Vehkaoja <sup>1</sup>

<sup>1</sup>Department of Automation Science and Engineering, Tampere University of Technology, Tampere, Finland

<sup>2</sup>Department of Electronics and Communications Engineering, Tampere University of Technology, Tampere, Finland

vala.jeyhani@tut.fi

+358400403839

## Abstract

Respiration rate (RR) is considered as a useful parameter in characterizing the health condition of a person. Among the methods used for respiration measurement, Electrical Impedance Pneumography (EIP) can be easily obtained in wearable applications due to the possibility of using the electrocardiography (ECG) electrodes for the EIP measurement. In the fast growing field of wearable devices, having clinically valuable and reliable information along with providing the convenience of the user, is probably the most important and challenging issue. To address the need of small sized devices for ECG (and EIP) measurements, EASI electrode configuration is an acceptable solution. The signals from EASI system not only provide useful information by themselves when directly used for cardiological analyses, but can also be converted to the standard 12-lead ECG information. With aforementioned advantages of EASI system, the question then arises how suitable the electrode locations of the system are for EIP measurements and what algorithms perform better for respiration rate derivation. In this work, we evaluated eight methods for deriving respiration rate from EIP signals measured from 15 subjects (10 males + 5 females) in three conditions: standing, walking slowly, and walking fast. The algorithms were autoregressive (AR) modeling (three different approaches), Fast Fourier Transform (FFT), autocorrelation, peak detection and two counting algorithms. Our results show that *advanced counting method* is the most promising approach among the ones studied in this work. For this algorithm, the concordance correlation coefficients of the respiration rate estimates between EIP and the reference measurement were 0.96, 0.90 and 0.97 for standing, walking with 3 km/h speed, and walking with 6 km/h speed respectively.

## Keywords

Electrical impedance pneumography, respiration cycle length, respiration rate, wearable

## Conflict of Interest

The authors declare that they have no conflicts of interest.

## Introduction

Wearable electronic devices are becoming more and more popular especially in sports, wellbeing, and entertainment applications. In addition to these consumer applications, wearable body monitoring, combined with wireless data transmission and real-time analysis in the cloud is a good example scenario of digitalized healthcare. Continuous patient monitoring, assessment, and automatic alarm generation enable early discharge and early intervention in case of complications thus decreasing healthcare costs and improving the quality of care.

Pulmonary measurement and especially monitoring of respiration rate (RR) is a very useful tool in characterizing the physiological condition of a person in both clinical and well-being applications. Many different measurement methods can be used for acquiring the respiration information. Spirometry, which directly measures the flow rate of the breathing air is the gold standard monitoring technique and provides the most accurate pulmonary information. Estimating different parameters of the breathing airflow such as temperature, humidity and CO<sub>2</sub> provides alternative techniques for this purpose. The temperature can be measured by using a nasal or oronasal thermistor [1] or infrared thermography [2]. Monitoring the pressure is another approach [3] and it can be performed by different tools such as mouthpiece or facemask and it has been validated for use at least in adults [4]. Inductance pneumography [5], electrical impedance pneumography (EIP) [6], capnography [7], and using other physiological signals such as Electrocardiography (ECG) [8] and Photoplethysmography (PPG) [9] are other methods which have been studied and used for respiration monitoring. A comprehensive review about different methods for respiration measurements has been written by AL-Khalidi et al. [10].

From the aforementioned methods, the ones that require the sensor to be located in the facial area have usability limitations and cause inconvenience for the user, especially in ambulatory applications. On the other hand, using EIP provides some benefits comparing to others. For on-body physiological monitoring that incorporates ECG measurement, EIP can be measured from the same electrodes as ECG thus avoiding the need to include additional sensors worn by the user. Recent interest has been towards flexible and stretchable physiological monitoring devices manufactured with printing technologies [11]. In this case, EIP measurements for acquiring respiration information is a suitable choice.

The EIP signals can provide vital pulmonary information such as respiration cycle length (RCL), rhythm and tidal volume [6]. Various signal processing methods have been proposed for estimating the respiration rate from signals recorded with aforementioned sensor modalities. The Fast Fourier Transform (FFT) has been used by Pimentel et al. [12] and Karlen et al. [13] for extracting the respiration rate from blood pressure and PPG signals, respectively. Autoregressive (AR) modeling of the signal is also a widely used method for estimating the respiration rate and various approaches are used for selecting the respiration component from the model. In the area of ECG derived respiration (EDR), Johnson et al. considered the pole with the smallest angle, which is selected after removing the poles which are located out of the respiration rate range or have a magnitude smaller than the 95<sup>th</sup> percentile [14]. The same approach is used in another study for estimating respiration rate from PPG [15]. Fleming et al. used the pole with the magnitude closest to the unit circle for estimation of the breathing rate from photoplethysmogram [16]. Autocorrelation function (ACF) has also been utilized for deriving the respiration rate. Sun and Matsui considered the first peak after the midpoint of the ACF as the respiration rate from Doppler Radar signals [17]. In addition, Bettermann et al. introduced a counting method which was based on counting prominent oscillations originating from respiratory activity [18]. This method was then improved by Schäfer and Kratky [19].

These different methods have been applied on various types of physiological signals, which carry respiration information and are mostly studied with databases that feature measurements in stable conditions. Therefore, the question is still unanswered that what is the best estimator for derivation of respiration rate from EIP signals in case of having movement artifacts, which is often the case with wearable devices used in ambulatory monitoring. Additionally, the feasibility, accuracy, and stability of using EIP monitoring in ambulatory applications that are

The final publication is available at Springer via <https://doi.org/10.1007/s12553-016-0156-0>

considered in the clinical (and not only the well-being) area and are accompanied by physical activities, are not confirmed yet.

Unobtrusiveness is a key requirement for wearable monitoring intended for long-term use and therefore having a small-sized device is of high importance. EAS electrode setup, a sub-set of EASI setup [20], is a small area electrode configuration, which can improve the usability of wearable devices. In this configuration, the electrodes E, A and S are located at the lower part of the sternum, the V5 electrode location of the standard 12-lead ECG, and at manubrium, respectively. In previous work, we explored the usability of EAS electrode configuration for EIP measurement and concluded that A-S electrode pair provides the best signal for the breathing rate estimation [21]. As an extension to the previous work, we have now evaluated eight different signal processing methods for deriving respiration rate with 15 subjects (10 males + 5 females) in three conditions: standing, walking with 3 km/h speed and walking with 6 km/h speed, using the A-S electrode pair for the EIP measurement.

Since the wearable devices are usually limited in computational power, clock frequency and battery capacity, the complexity of the processing algorithms, including respiration rate estimation, has a great impact on the system. Therefore, the considered methods are simple techniques that can be implemented in embedded devices, having a small influence on their limited available resources. Additionally, the preprocessing steps are kept as simple as possible. The considered methods are simple peak detection, autocorrelation, FFT, AR model (three different approaches), and two counting methods.

The outline of this paper is organized as follows. In section II, the measurement procedure, RR detection algorithms and statistical evaluation strategies are described. The results are shown and discussed in section III. Finally, some concluding remarks are given in section IV.

## Methods

Totally 17 subjects participated in this study. Two of them were later excluded from the data analyses due to problems in the measurement hardware i.e. damaged measurement cables caused random distortions to the signal. The characteristics of the remaining 15 subjects (10 male and 5 female) are shown in Table 1. None of the participants reported having pulmonary problems. Skin preparation was performed for all the subjects prior to applying the recording electrodes. This procedure included shaving the chest hair in the area of the electrode locations, cleaning the skin with alcohol and removing dead skin cells by scraping off with a rough sponge. Informed consent was obtained from all individual participants included in the study. The electrode wires were attached to the body by a piece of adhesive tape to eliminate the effect of the wire movements on the measurements.

Table 1 Subjects' characteristics

	N (%) or mean $\pm$ SD	Range
Sex (male)	66 %	—
Age (years)	29.4 $\pm$ 5.2	23 – 38
Weight (kg)	70.4 $\pm$ 13.4	47 – 94
Height (cm)	172.3 $\pm$ 8.1	157 - 186
Body mass index	23.6 $\pm$ 3.5	19.1 - 31

The measured signals included flow thermography, impedance pneumography, and two channels of ECG, which were only used for data synchronization. The test procedure included three phases: standing, walking slowly with 3km/h speed and walking fast with 6km/h speed. The duration of each test phase was 5 minutes excluding transition between the phases. The parts that involved walking were measured on a treadmill. The measurements for the three phases were done continuously and separated from each other afterwards according to annotations inserted in the data during the measurement. The measurement procedure was the same for all the subjects.

## Measurements Setup

Two separate devices were employed in this study to acquire the signals. The first device, which featured an ADS1292R analog front-end component (AFE) from Texas Instruments and an AVR microcontroller from ATMEL, was used to measure the impedance pneumography signal and one channel of ECG. The EIP signal was measured using two-electrode configuration. The same electrodes were used for the ECG recording. The acquired signals along with sample numbers were transmitted to a computer through a USB connection. A graphical user interface (GUI) was designed to monitor the signals and record an annotation signal, which was used to mark the beginning of each test phase. The signals were sampled at 500 Hz frequency and digitized with 24-bit resolution. The modulation signal used for the EIP measurement was internally generated by the AFE and had a frequency of 32 kHz and a phase of 112.5°. The gain of the preamplifiers was set to 6 for both signals. The two measurement electrodes were placed on the S and A electrode locations of the EASI electrode configuration.

The second device was used to record flow thermography (FTG) signal that was used to calculate the reference respiration rate. Single lead ECG (standard lead II) was also recorded with the second device to be able to ensure the data synchronization between the two devices. The sampling frequency was set to 500 samples per second for both channels. The flow thermography was acquired utilizing an NTC thermistor placed inside a mask that was worn in front of the mouth and the nostrils during the test.

## Signal Pre-processing

All the signals were pre-processed before being evaluated by the respiration rate estimation algorithms. Pre-processing included three steps: synchronizing, filtering, and dividing into frames for processing by the respiration rate algorithms.

At the beginning of each subject's measurement, electrode wires were removed from both devices and reconnected at the same time. This event was then detected in preprocessing phase and was used as one of the marking points for the synchronization. The ECG signals were then processed by Pan-Tompkins R-peak detection algorithm [22] and resulting R-peak interval signals were compared to verify exact synchronization throughout the whole recording.

The range of respiration rate was assumed to be within the range of 4 to 60 breath per minute (bpm) similarly as in [12, 23]. Narrower ranges such as 6 – 30 bpm [19, 24] and 6 – 60 bpm [25] have been used in some of the previous studies, but this consideration would eliminate the preservation of the respiration components e.g. in some clinically important conditions. Thus, both EIP and flow thermography signals were filtered by a 3<sup>rd</sup> order Butterworth high-pass filter with cut-off frequency of 0.06 Hz (corresponding to 4 bpm) and a 3<sup>rd</sup> order Butterworth low-pass filter with cut-off frequency of 1 Hz (corresponding to 60 bpm). Filtering was done using forward-backward technique to avoid any signal distortion that would have otherwise been caused by the non-linear phase response of the IIR-filter. The panels (a) and (b) in Fig. 1, Fig. 2 and Fig. 3 show examples of the filtered signals measured in the first, second, and third phase of the measurements, respectively.

For each subject, the beginning of each phase was annotated using the GUI during the measurement process. After filtering the signals, three 5-minute frames were extracted which correspond to standing, walking with 3km/h speed and with 6 km/h speed. Next, each 5-minute frame was divided into 58 15-second long frames with 10 seconds overlap (one frame every 5 second). Consequently, 870 frames from EIP and the reference signals were prepared in each phase to be analyzed by the rate estimation methods.

## Respiration Rate Algorithms

Eight approaches were evaluated for extracting the RR from the EIP signals. The evaluated algorithms were: simple peak detection, autocorrelation, FFT, AR model (three different approaches), and two counting methods. The principle of operation of each algorithm is described in the following. Most of these algorithms were previously proposed in the literature for RR estimation but the signal source, i.e. the sensor used in the measurement has varied and the methods have not been compared with each other for the EIP signals earlier.

### Time Domain Estimators

*Peak Detection:* For each frame, local maxima in the signal were detected and then the average of horizontal distance of consecutive maxima was calculated. This value divided by the sampling frequency and multiplied by 60 was reported as the respiration rate in bpm. The criteria for the peak detection algorithm was to have minimum horizontal distance of 1 second (according to the upper limit considered for the respiration range) and a positive amplitude. Ideally, the peaks in the respiration signal correspond to the point where the inhaling ends and exhaling starts. **Fig. 1** (a) and (b) show a 15-second frame of the reference signal and its corresponding EIP frame, respectively. **Fig. 1** (b) also illustrates the procedure of peak-detection estimator. The average of  $t_1$ ,  $t_2$  and  $t_3$  is considered as the period of the signal. The function was written so that it outputs NaN (Not a Number) when no peak was detected with the specified criteria. The number of NaNs (for EIP signals) are considered as a comparison factor between the algorithms. This simple approach has been mentioned by Charlton et al. [26] as one of the methods for RR estimation from ECG and PPG signals and it basically assumes a clean respiration signal with no distortions.

*Autocorrelation:* The autocorrelation sequence of a periodic signal has the same cyclic behavior as the signal itself. Autocorrelation function ( $r(\tau)$ ) is defined as

$$r(\tau) = \sum_{n=0}^{N-1-\tau} x(n)x(n + \tau) \quad (1)$$

in which  $x(n)$  represents the signal and  $N$  is the number of samples. After removing the left symmetric part of  $r(\tau)$ , the first peak can be considered as the component describing the periodicity of  $x(n)$ . This method is widely used for respiration rate estimation from different physiological signals in literature [17, 19]. In this study, the only criteria for the peak detection was the minimum horizontal distance, which was set to 1 second. The lag of the first peak after the midpoint of the autocorrelation function multiplied by  $60/f_s$  ( $f_s$  being the sampling frequency) was reported as the respiration rate in bpm. **Fig. 1** (c) depicts the right half of the autocorrelation function calculated from the EIP signal (shown in **Fig. 1** (b)) and the first peak detected ( $t_4$ ) as the estimate of the respiration cycle length. The method was designed to output a NaN if no peak (with the specified criteria) was detected.

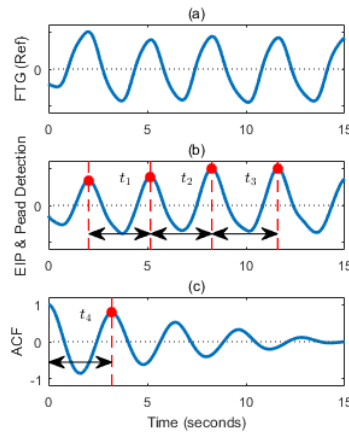


**Fig. 1** One frame of the reference signal (a) and its corresponding EIP frame (b) in the standing condition. The panel (b) also shows the output of the peak-detection estimator on the EIP signal. The panel (c) illustrates the autocorrelation of the EIP signal and the RCL estimated from it.

*Original Counting:* The two counting methods considered in this study try to remove the wrong extrema in the signal. In the Original counting [18] method, first a threshold is defined as  $0.2 \times Q_3$ , in which  $Q_3$  is the third quartile (75<sup>th</sup> percentile) of all local maxima ordinate values. The parts of the signal with two following conditions are considered as the respiration cycle:

- The part must begin and end at local maxima which are located above the threshold
- The part must contain exactly one minimum below zero and no other extrema in the region.

The average of the detected respiration cycles is reported as the RCL of the frame. One of the drawbacks of this algorithm, which is also discussed in [19], is that it frequently ignores cycles of breathing even when they are valid. Fig. 2 (b) and (c) illustrate the procedure of this algorithm. It can be seen that only one cycle is detected, which in this example is even not a correct cycle. This drawback is fixed in another algorithm proposed by Schäfer et al. in 2008 [19], which is called *advanced counting*.

*Advanced Counting:* In this method, a threshold is defined as the third quartile of the absolute values of vertical distances of the subsequent extrema, multiplied by 0.1. Then iteratively, the minimum value of the vertical differences is found, compared with the threshold, and both of its corresponding extrema are removed if the

difference is lower than the threshold. The average of the detected cycle lengths is reported as the RCL of the frame. Fig. 2 (d) shows the result of the algorithm. It can be seen that most of the cycles are detected correctly although one cycle ( $t_4$ ) is wrongly considered as a respiration cycle. The average of  $t_1, t_2, \dots, t_5$  is reported as the RCL of the frame

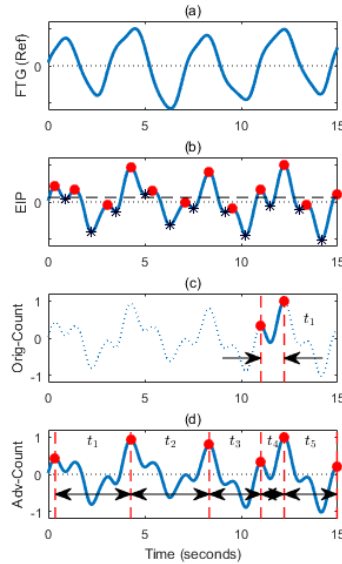


**Fig. 2** One frame of the reference signal (a) and its corresponding EIP frame (b) measured in walking with speed of 3 km/h. The panel (b) shows also the extrema of the signal which are used by the two counting methods. The dashed horizontal line shows the calculated threshold in the original counting method. The panel (c) pictures the only estimated respiration cycle by the original counting method. The panel (d) illustrates the considered respiration cycles by the advanced counting method.

### Frequency Domain Estimators

An evident approach for estimating the respiration rate is to locate the most prominent component in the frequency domain. Both Fast Fourier Transform (FFT) and Autoregressive model (AR) methods have been used in literature for estimating the spectrum of the respiration (directly measured or extracted from other physiological signals). Three different approaches, which have previously been used in literature for locating the pole in the AR model that corresponds to respiration frequency are explained in following in addition to one FFT-based method.

*FFT*: in this method, first, the signal was decimated to 4 samples per second (sps) to improve the spectrum resolution. Then, the FFT of the signal was calculated with 1024 bins and the first quarter of it was kept. As a result, the frequency resolution was 1/256 Hz in the range of 0 to 1 Hz. Finally, the peaks of the spectrum were detected and the frequency of the maximum peak was considered to be related to the respiration rate in that frame. Fig. 3 (c) illustrates the result of the FFT and the calculated frequency  $f_1$ .

*AR Model*: After decimating the signal to 4 sps, it was modeled by an autoregressive (AR) all-pole model using Burg's method [27]. The order of the model was chosen to 15. This value was chosen experimentally, although similar values are reported in similar works such as [19]. Various approaches for choosing the respiration pole have been used in the literature. In this study, the following three methods are considered.

- *Minimum-angle-pole (AR - MAP)*: First, the poles which were out of the respiration range were excluded. Then a threshold was calculated as the 95<sup>th</sup> percentile of the magnitude of the remaining peaks and smaller ones were removed. Finally, the peak with smallest angle was considered as the respiration pole [14, 15].

- *Maximum-magnitude-pole (AR-MMP)*: After removing the out-of-range poles, the angle of the one with the largest magnitude was considered as the respiration frequency [16]. The frequency  $f_2$  in Fig. 3 (d) is the maximum magnitude pole of the AR model resulted from the EIP signal shown in Fig. 3 (b).
- *Maximum-peak (AR - MP)*: In this approach, first the frequency response of the model was calculated (with 512 points) and then the maximum peak in the spectrum was chosen as the dominant respiration frequency ( $f_3$  in Fig. 3 (d) and (e)). We have not seen this method being applied for RR estimation in the literature.

The reason for considering AR – MP is that the real frequency response of the system modeled by autoregressive model is affected by all of the poles. More specifically, the frequency response  $H(\omega)$  is calculated as

$$H(\omega) = \prod_{n=1}^P d_{p(n)} / \prod_{n=1}^Z d_{z(n)} \quad (2)$$

in which  $P$  and  $Z$  show the number of poles and zeros in the system, respectively.  $d_{p(n)}$  and  $d_{z(n)}$  are the distance of the frequency  $\omega$  (a point on the unit circle for which the  $H(\omega)$  is calculated) and the  $n$ -th pole and zero, respectively. For an all-pole model, the distance between the zeros at all the frequencies is unity. Therefore, the denominator in the equation (2) can be removed. In Fig. 3 (e), it can be seen how the magnitude of the poles, which are located close to unit circle, is translated to the magnitude frequency response of the system.

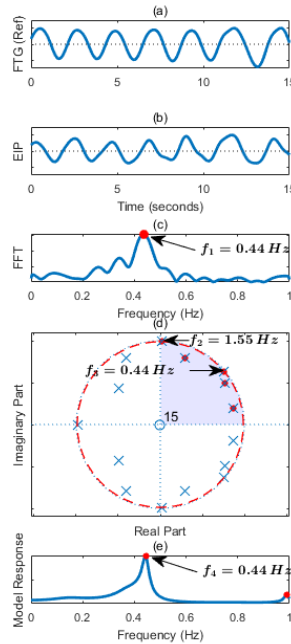


**Fig. 3** One frame of the reference signal (a) and its corresponding EIP frame (b) measured in walking with speed of 6 km/h. The third panel (c) shows the result of the FFT method. The panel (d) shows the result of modeling the signals by an autoregressive model with an order of 15. The dashed red line shows the threshold calculated when considering the pole with the smallest angle. The shaded region shows the respiration range. The frequency  $f_2$  shows the angle of the pole with largest magnitude and also the pole with smallest angle (after applying the threshold). The frequency  $f_3$  shows the frequency of the maximum peak found in the frequency response of the model (bottom diagram (e)).

## Statistical Analysis

For studying and comparing the performance of the respiration rate estimators, the lack of a gold standard reference measurement method impedes straightforward analysis and conclusion. Identifying the parts of the reference

respiration signal from which the respiration rate cannot be unambiguously defined, e.g. due to disturbances in the signal or large variation in the respiration cycle lengths, is challenging and imposes uncertainty on the results. To address this problem, we first ran a statistical test between the methods applied only on the reference signals measured from all the subjects and only in the standing condition. The results show that the Count-adv shows the best correlation with the other methods. We used this estimator along with the AR – MP method for finding the nonstationary frames in the reference signals. The two estimators were applied on the reference signals and the frames were preserved if the difference between the two estimated RRs by the two algorithms was smaller than 3 bpm. One of the advantages of using these two methods is that one of them is implemented in frequency domain and the other operates in time domain. Therefore, most probably the nonstationary frames that are treated differently by the time- and frequency-domain estimators are selected and removed in the final analysis. **Fig. 4** shows the Pearson’s correlation coefficient between the methods applied on the reference frames.

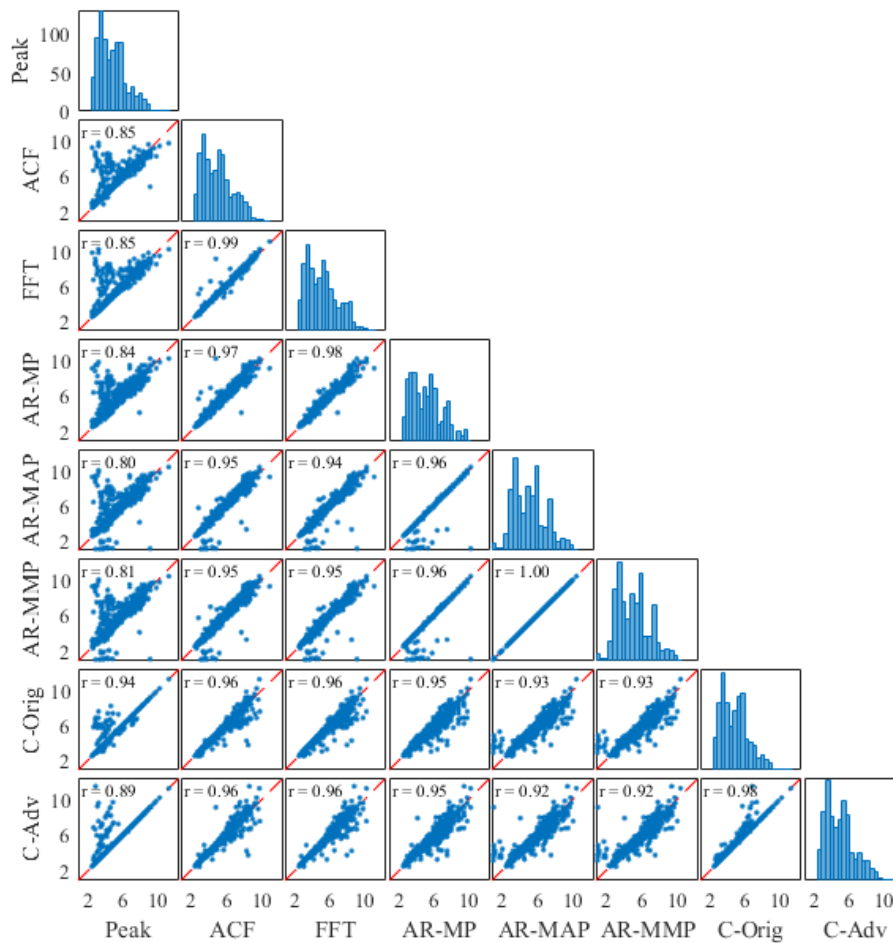


**Fig. 4** The correlation between methods when applied on the reference signals measured from all the subjects in the standing condition. The number in each panel is the Pearson correlation coefficient between the results of the two methods. The method used in each panel is mentioned at the leftmost and bottom side of the corresponding row and column, respectively. The bar plots depict the histogram of the RRs produced by each method. The x-axis and y-axis range of all scatter plots and the x-axis range of bar plots are the same. The y-axis range for all the histograms is [0, 131].

In the final analysis, the results were analyzed by the mean absolute error (MAE), the mean error (ME) and the mean absolute percentage error (MAPE). MAE is defined as

$$MAE = \frac{1}{N} \sum_{n=1}^N |\hat{y}[n] - y[n]|, \quad (3)$$

the mean error as

$$ME = \frac{1}{N} \sum_{n=1}^N (\hat{y}[n] - y[n]), \quad (4)$$

and MAPE (in percentage) as

$$MAPE = \frac{1}{N} \sum_{n=1}^N \frac{|\hat{y}[n] - y[n]|}{y[n]} \times 100, \quad (5)$$

where  $\hat{y}$  and  $y$  indicate the EIP and flow signals, respectively. Additionally, to evaluate the linear dependency between respiration rates estimated from the EIP and the reference signals, the *concordance correlation coefficient* [28] ( $r_c$ ) was included in the evaluations. The coefficient  $r_c$  is defined as

$$r_c = \frac{2s_{y\hat{y}}}{s_y^2 + s_{\hat{y}}^2 + (\bar{y} - \bar{\hat{y}})^2} \quad (6)$$

in which  $\bar{\hat{y}}$  and  $\bar{y}$  indicate the average of the data points in  $y$  and  $\hat{y}$ , respectively.  $s_y^2$  is the variance of  $y$  and  $s_{y\hat{y}}$  is the covariance.

## Results and Discussions

The level of noise and the amount of movement artefacts in the EIP signal varied considerably between the subjects and obviously also between the test phases. The two first diagrams in Fig. 1, Fig. 2 and Fig. 3 in the previous section show examples of one frame of reference signal and its corresponding frame of EIP in standing, walking with 3 km/h speed and walking with 6 km/h speed, respectively. It can be seen that the reference signal is clean in all the phases. On the other hand, it is noticeable how the EIP signal is affected by movement artifacts. It is worth mentioning that the EIP signal looks cleaner in the third phase comparing to the second one, since most of the artifacts are located outside of the desired frequency range and are thus filtered out.

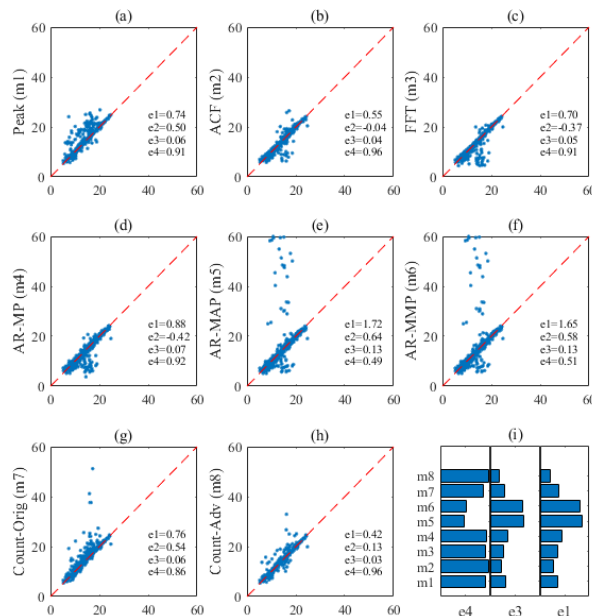
There were totally 870 frames for EIP and reference signals in each phase. The phases were studied separately to be able to see how the movement artifact caused by walking impairs the respiration rate estimation. The reference signals were processed by Count-adv and AR – MP methods and the frames were preserved only if the difference between the results of the two algorithms was smaller than 3 bpm. The total number of frames removed for standing, walking with 3 km/h speed and, walking with 6 km/h speed were 9, 13 and 7, respectively. In the final evaluation, the RR values provided by the Count-adv method were used as the reference in all the cases.

Fig. 5, Fig. 6 and Fig. 7 show the comparison of the first, second, and third test phases, respectively. Each figure shows a group of scatter plots that indicate how well the RR results of different methods correlate with the reference. In all the figures, the horizontal axis presents the reference respiration rate values (in bpm). The statistical results are calculated after removing the NaN values. In these figures, the errors e1, e2, e3 and e4 correspond to MAE, ME, MAPE and concordance correlation coefficient ( $r_c$ ), respectively.

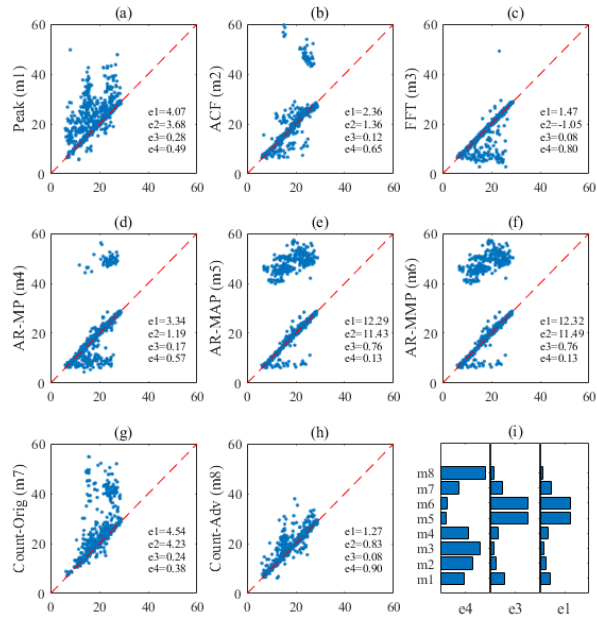
In Fig. 5, which presents the results in the standing phase, it can be seen that  $r_c$  is above 90% for all the methods except AR – MMP and AR – MAP. The best performance is achieved with ACF and Count-adv estimators. The number of missing frames by these two methods is 0 and 8, respectively.

Fig. 6 shows the results for the second phase of the measurements. It is noticeable that all three AR approaches are confused by the high frequency components in the model which are either related to the respiration harmonics or the in-range movement artifacts. The advanced counting method has the best performance. The mean absolute error is 1.27 bpm for this method. Only 8 frames (out of 857, 13 frames were removed in pre-processing) were missed by this estimator in the second phase of the measurement.

Fig. 7 depicts the results for the last phase of the measurement. The AR model approaches based on the angle and magnitude of the poles (MAP and MMP) are confused by higher frequency components. The best performance is provided by the advanced counting method with  $r_c$  of 0.97. It is worth mentioning that since the movement artifacts in the third phase are mostly located out of the respiration range, the error in this phase is smaller (for almost all the methods) comparing to the second phase. Even though the amplitude of the movement artifacts in the raw EIP signal (before preprocessing) is considerably larger during intensive, fast walking with 6 km/h speed.



**Fig. 5** The comparison of the results in the first phase of the measurements (standing). The unit for both x and y axes is breath per minute. Name of each method is mentioned in label of the y axis. The horizontal axis represents the results from the reference signal for all the plots. The errors  $e1$ ,  $e2$ ,  $e3$  and  $e4$  show MAE (bpm), ME (bpm), MAPE, and concordance correlation coefficient, respectively. The panel on the bottom right (i) shows a comparison between the errors (excluding ME) for the eight methods.



**Fig. 6** The comparison of the results in the second phase of the measurements (walking with 3 km/h speed). The unit for both x and y axes is breath per minute. Name of each method is mentioned in label of the y axis. The x axis represents the results from the reference signal for all the plots. The errors  $e1$ ,  $e2$ ,  $e3$  and  $e4$  show MAE (bpm), ME (bpm), MAPE, and concordance correlation coefficient, respectively. The panel on the bottom right (i) shows a comparison between the errors (excluding ME) for the eight methods.

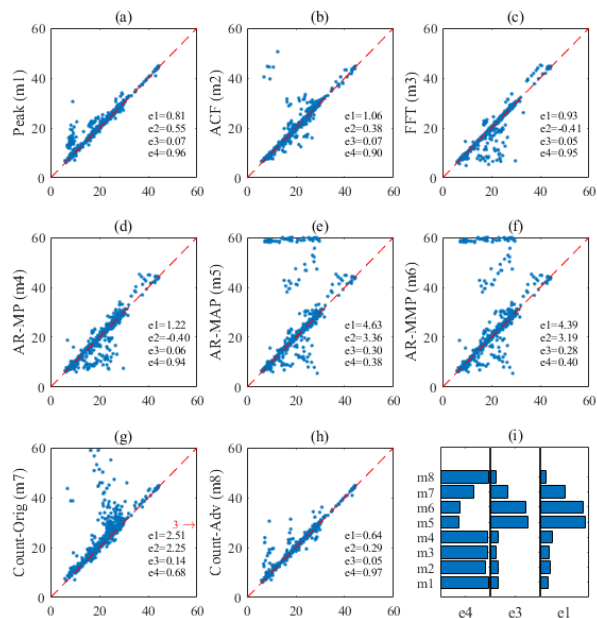


**Fig. 7** The comparison of the results in the third phase of the measurements (walking with 6 km/h speed). The unit for both x and y axes is breath per minute. Name of each method is mentioned in label of the y axis. The x axis represents the results from the

reference signal for all the plots. The small red arrow and the number beside it at the right side of the plots show the number of points which are located out of the horizontal axes range (which is according to the respiration rate range). The errors e1, e2, e3 and e4 show MAE, ME, MAPE and concordance correlation coefficient, respectively. The panel on the right bottom shows a comparison between errors (excluding ME) for the eight methods.

The number of discarded frames by the algorithms another performance feature for the algorithm comparison in this study. The criteria for neglecting a frame are considered differently in the studied methods. For instance, the search criteria of the peak detection procedure can result in zero or only one peak in the frame and therefore eliminate the possibility to calculate the period. It is worth noting that having some parts of the data discarded by an algorithm is not necessarily a drawback if the algorithm has been designed so that it does not report any value if the signal quality is poor and the estimate is therefore considered unreliable. **Error! Not a valid bookmark self-reference.** shows the number of discarded frames by each algorithm and in each phase of the measurement. As seen in Table 2, original counting method has discarded a large number of frames (382 out of 2581) and still its estimation results are poor. The same applies to AR-MAP method.

**Table 2** Number of EIP frames discarded by different methods in the three measurement phases

Method	Standing	Walking – 3 km/h	Walking – 6 km/h
Peak	9	2	0
ACF	0	0	0
FFT	0	0	0
AR – MP	0	0	0
AR – MAP	76	50	81
AR – MMP	0	0	0
Count – Orig	112	174	96
Count – Adv	8	8	3

**Table 3** The agreement between EIP and reference measurement for male and female subjects separately. The advanced counting method is used for the EIP frames.

Table 3 displays the errors and the concordance correlation coefficients resulted by the best performing method, advanced counting method for male and female subjects, separately. In both of the groups, the second phase (walking with 3 km/h speed) is clearly the most challenging measurement condition. With this set of data, the accuracy has been clearly better for female subjects, although the relatively small number of test subjects prevents drawing conclusions about gender specific differences in the accuracy.

Sex	Male			Female		
	Standing	Walking 3 km/h	Walking 6 km/h	Standing	Walking 3 km/h	Walking 6 km/h
MAE (bpm)	0.52	1.53	0.78	0.23	0.75	0.35
ME (bpm)	0.18	1.06	0.40	0.02	0.39	0.10
MAPE (%)	4.41	10.6	6.33	1.70	3.33	1.55
$r_c$	0.95	0.84	0.95	0.99	0.95	1.00

## Conclusion

In this work, we evaluated eight methods including AR model (three approaches), Fast Fourier Transform, autocorrelation, simple peak detection and two counting algorithms for estimation of respiration rate from Electrical Impedance Pneumography recordings. Totally, 17 subjects (10 male and 7 female) participated in this study, among which, two were excluded due to problems in the measurement hardware. There were three phases in the measurements: standing (in which the subjects were almost still), walking with 3 km/h and 6 km/h speeds. Along with EIP signals, flow thermography was measured and used as the reference for the comparisons.

Our results show that the average respiration rate for 15 second windows can be estimated accurately from the EIP signal measured from the A-S electrode pair. From the evaluated methods, advanced counting method introduced by Schäfer and Kratky [19] performed the best. For this algorithm, the concordance correlation coefficients of the respiration rate estimates between EIP and the reference measurement were 0.96, 0.90 and 0.97 for standing, walking with 3 km/h speed, and walking with 6 km/h speed, respectively. Most of the methods (except two approaches based on the AR model) performed well when there was little or no artifacts in the signals (standing condition). The most challenging phase of the measurement was the second phase (walking with 3 km/h speed) since the movement artifacts are located in the same frequency range as what is considered for the respiration, i.e. up to 1 Hz even though the raw signals measured in the third phase (walking with 6 km/h speed) seemed to be more corrupted by the artifacts. In the second phase, all the AR-model approaches were misled by either the respiration harmonics or the movement artifacts and RR was often overestimated. The FFT method, on the other hand, often underestimated the RR. Therefore, we conclude that the frequency-domain methods performed poor when the measurement is accompanied by physical activities, as has been reported in similar studies [19].

Making conclusions about the feasibility of implementing these algorithms in wearable devices can be challenging due to different architectures of the integrated circuits, e.g. availability of FFT hardware accelerator (HWFFT), different programming styles (e.g. for peak detection algorithm) and restrictions imposed by the application requirements. However, the best performing algorithm in this study (advanced counting) is clearly free of complex mathematical computations. Therefore, this algorithm should be a suitable choice for most of the low-power embedded platforms. Due to the same concern, the preprocessing block, which has a significant effect on the presence of unwanted elements in the signal, has been kept simple and is limited to filtering.

The lack of a gold standard method for estimating the true respiration was one of the challenges in this study. Nonstationary respiration during a single frame of signal may cause large errors since different algorithms treat this issue differently and report disparate results.

Future work will focus in enhancing the methods and further analysis of the source of errors. The effect of non-regular movement artifacts will also be studied. The influence of flexible electrodes having integrated cables attached to the body, as presented in [11], on EIP measurement and especially to the movement artifacts will also be examined. In addition, we will extend the measurements to a larger population with wider demographic distribution. Experiments will be performed in ambulatory conditions to gain insight into real-life performance of RR monitoring and its probable problems.

## Acknowledgement

The authors would like to thank all the volunteer subjects. This research was funded by the Finnish Funding Agency for Innovation (Tekes) and several Finnish companies as a part of VitalSens project. Funding decision number: 40103/14. M. Mäntysalo is supported by Academy of Finland (grant no. 288945 and 294119).

## Ethical Considerations

All procedures performed in studies involving human participants were in accordance with the ethical standards of the institutional and/or national research committee and with the 1964 Helsinki declaration and its later amendments or comparable ethical standards.

## References

1. Verginis N, Davey MJ, Horne RSC. Scoring respiratory events in paediatric patients: Evaluation of nasal pressure and thermistor recordings separately and in combination. *Sleep Med.* 2010;11(4):400–5.
2. Abbas AK, Heimann K, Jergus K, Orlikowsky T, Leonhardt S. Neonatal non-contact respiratory monitoring based on real-time infrared thermography. *Biomed Eng Online.* 2011; doi:10.1186/1475-925X-10-93
3. Shneerson, JM. *Sleep medicine: a guide to sleep and its disorders.* John Wiley & Sons; 2009.
4. Thurnheer R, Xie X, Bloch KE. Accuracy of nasal cannula pressure recordings for assessment of ventilation during sleep. *Am J Resp Crit Care.* 2001;164(10):1914–9
5. Hill SL, Blackburn JP, Williams TR. Measurement of respiratory flow by inductance pneumography. *Medical and Biological Engineering and Computing.* 1982;20(4):517–8.
6. Freundlich JJ, Erickson JC. Electrical impedance pneumography for simple nonrestrictive continuous monitoring of respiratory rate, rhythm and tidal volume for surgical patients. *Chest Journal.* 1974;65(2):181–4
7. Von Schéeleand BHC, Von Schéeleand IAM. The measurement of respiratory and metabolic parameters of patients and controls before and after incremental exercise on bicycle: supporting the effort syndrome hypothesis? *Appl Psychophys Biof.* 1999; doi:10.1023/A:1023484513455
8. Mirmohamadsadeghi L, Vesin JM. Respiratory rate estimation from the ECG using an instantaneous frequency tracking algorithm. *Biomed Signal Proces.* 2014;14:66–72.
9. Leonard PA, Douglas JG, Grubb NR, Clifton D, Addison PA, Watson JN. A fully automated algorithm for the determination of respiratory rate from the photoplethysmogram. *J Clin Monitor Comp.* 2006; doi:10.1007/s10877-005-9007-7
10. AL-Khalidi FQ, Saatchi R, Burke D, Elphick H, Tan S. Respiration rate monitoring methods: a review. *Pediatr Adol.* 2011; doi:10.1002/ppul.21416
11. Vuorinen T, Vehkaoja A, Jeyhani V, Nojonen K, Onubeze A, Kankkunen T, Puuronen AK, Nurmentaus S, Preejith SP, Joseph J, Seppänen T, Sivaprakasam M, Mäntysalo M. Printed, Skin-Mounted Hybrid System for ECG Measurements. *Proc. 6th Electronics System-Integration Technology Conference.* 2016.
12. Pimentel MAF, Santos MD, Arteta C, Domingos JS, Maraci MA, Clifford GD. Respiratory rate estimation from the oscillometric waveform obtained from a non-invasive cuff-based blood pressure device. *Eng Med Biol Soc Ann.* 2014; doi:10.1109/EMBC.2014.6944456
13. Karlen W, Raman S, Ansermino JM, Dumont GA. Multiparameter respiratory rate estimation from the photoplethysmogram. *IEEE T Bio-Med Eng.* 2013; doi:10.1109/TBME.2013.2246160
14. Johnson AEW, Cholleti SR, Buchman TG, Clifford GD. Improved respiration rate estimation using a Kalman filter and wavelet cross-coherence. *Computing in Cardiology.* 2013;791–794.
15. Fleming SG, Tarassenko L. A comparison of signal processing techniques for the extraction of breathing rate from the photoplethysmogram. *International Journal of Biological and Medical Sciences.* 2007;2(4):232–6.
16. Fleming S, Tarassenko L, Thompson M, Mant D. Non-invasive measurement of respiratory rate in children using the photoplethysmogram. *Eng Med Biol Soc Ann.* 2008; doi:10.1109/IEMBS.2008.4649554
17. Sun G, Matsui T. Rapid and stable measurement of respiratory rate from Doppler radar signals using time domain autocorrelation model. *Eng Med Biol Soc Ann.* 2015; doi:10.1109/EMBC.2015.7319755
18. Bettermann H, Engelke P, Van Leeuwen P, Heckmann C. Determination of Respiratory Rate on the Basis of Respiratory Sinus Arrhythmia (in German). *Biomed Tech.* 1996; doi:10.1515/bmte.1996.41.11.319
19. Schäfer A, Kratky KW. Estimation of breathing rate from respiratory sinus arrhythmia: comparison of various methods. *Ann Biomed Eng.* 2008; doi:10.1007/s10439-007-9428-1

20. Dower GE, Yakush A, Nazzal SB, Jutzy RV, Ruiz CE. Deriving the 12-lead electrocardiogram from four (EASI) electrodes. *J Electrocardiol.* 1988; doi:10.1016/0022-0736(88)90090-8
21. Jeyhani V, Vuorinen T, Nojonen K, Mäntysalo M, Vehkaoja A. Optimal Short Distance Electrode Locations for Impedance Pneumography Measurement from the Frontal Thoracic Area. *XIV Mediterranean Conference on Medical and Biological Engineering and Computing.* 2016; doi:10.1007/978-3-319-32703-7\_222
22. Pan J, Tompkins WJ. A real-time QRS detection algorithm. *IEEE T Bio-Med Eng.* 1985; doi:10.1109/TBME.1985.325532
23. Pimentel MAF, Clifton DA, Clifton L, Tarassenko L. Probabilistic estimation of respiratory rate using Gaussian processes. *Eng Med Biol Soc Ann.* 2013; doi:10.1109/EMBC.2013.6610147
24. Vehkaoja A, Peltokangas M, Lekkala J. Extracting the respiration cycle lengths from ECG signal recorded with bed sheet electrodes. *J Phys Conf Ser.* 2013; doi:10.1088/1742-6596/459/1/012015
25. Dehkordi PKh, Marzencki M, Tavakolian K, Kaminska M, Kaminska B. Validation of respiratory signal derived from suprasternal notch acceleration for sleep apnea detection. *Eng Med Biol Soc Ann.* 2011; doi:10.1109/IEMBS.2011.6090950
26. Charlton PH, Bonnici T, Tarassenko L, Clifton DA, Beale R, Watkinson PJ. An assessment of algorithms to estimate respiratory rate from the electrocardiogram and photoplethysmogram. *Physiol Meas.* 2016;37(4):610.
27. Kay, Steven M. *Modern spectral estimation: theory and application.* Englewood Cliffs, NJ: Prentice Hall; 1988.
28. Lawrence I, Lin K. A concordance correlation coefficient to evaluate reproducibility. *Biometrics.* 1989; doi:10.2307/2532051